Residual stress estimation in ferroelectric $PbTiO_3$ thin films by Raman spectroscopy

A. Bartasyte,[1,2,*] S. Margueron,[3] J. Kreisel,[1] P. Bourson,[3] O. Chaix-Pluchery,[1] L. Rapenne-Homand,[1] J. Santiso,[4] C. Jimenez,[1] A. Abrutis,[2] F. Weiss,[1] and M. D. Fontana[3]

[1]*Laboratoire des Matériaux et du Génie Physique (CNRS UMR 5628), Minatec, Grenoble Institute of Technology, 3 Parvis Louis Néel, 38016 Grenoble, France*

[2]*Department of General and Inorganic Chemistry, Vilnius University, Naugarduko 24, LT-03225 Vilnius, Lithuania*

[3]*Laboratoire Matériaux Optiques, Photonique et Systèmes (CNRS UMR 7132), University of Metz and Supélec, 2 Rue E. Belin, 57070 Metz, France*

[4]*Centro de Investigación en Nanociencia y Nanotecnologia, CIN2 (CSIC-ICN), Campus de la UAB, E-08193, Bellaterra, Barcelona, Spain*

(Received 12 September 2008; revised manuscript received 22 January 2009; published 5 March 2009)

A comparative analysis of Raman spectra from polydomain $PbTiO_3$ thin films with both polydomain and single-domain $PbTiO_3$ crystals is presented. The Raman signature of ferroelectric thin films is complex when used for stress analysis. Raman spectroscopy of a stress-free polydomain $PbTiO_3$ single crystal reveals that the profile of phonon modes can be significantly modified by the existence of quasimodes. The different potential origins of quasimodes are discussed, and it is emphasized that quasimodes should be taken into account for an accurate estimation of residual stress values in ferroelectric films via Raman scattering. We finally propose and illustrate that the E(3TO) hard mode is more reliable for the estimation of biaxial residual stress in $PbTiO_3$ than the commonly used E(1TO) soft mode.

DOI: 10.1103/PhysRevB.79.104104 PACS number(s): 77.84.Dy, 78.30.−j

I. INTRODUCTION

Ferroelectric perovskite oxides receive considerable attention for their useful physical properties. Thus, studies of epitaxial ferroelectric thin films are of great interest because of their potential applications as elements in static random access memories, high-dielectric-constant capacitors, or optical waveguides.[1] An innovative way of varying physical properties of thin films is to use the interfacial strain when a film is deposited on a substrate. For example, it is known that in high-quality strained epitaxial films, the transition temperature can be shifted by a few hundred degrees[2–7] and it has been proposed that the primary and secondary order parameters can be decoupled.[4,5,8] We note that most of the work in the literature concerning strain effects on film properties does not present a direct measurement of the residual stress and results are generally assigned to theoretical stress values. Thus, simple methods to estimate the residual stress, such as x-ray diffraction (XRD) and Raman spectroscopy, are of special interest.

Ferroelectricity, and thus, Raman modes in ferroelectrics are strongly influenced by mechanical deformation of the sample resulting from, e.g., hydrostatic pressure or stresses.[9–15] Raman spectroscopy has been shown to be a valuable method to determine residual stresses in various materials and composite structures.[16–19] The relation between the Raman shift and stresses can be determined by different calibration methods, such as diamond-anvil cell pressure, XRD, and flexion methods.[20,21] However, before using the position of a Raman band for a stress analysis it is crucial to be sure that the analyzed position is truly related to stress and that the selected band in itself does allow a meaningful interpretation. It has already been pointed out that depolarization by domain structure and grain size effects on materials such as ferroelectrics, superconductors, and semiconductors should be taken into account.[22–24] However, a detailed description of the consequence of the domain structure and other potential pitfalls in a Raman stress analysis is still missing in the literature which has led to numerous misinterpretations.

By discussing in detail the Raman spectra of polydomain $PbTiO_3$ (PTO) thin films, we demonstrate that the analysis of the Raman signature of ferroelectric thin films is indeed complex with regard to a stress analysis. We show (i) that the comparative analysis of the thin film Raman signature with that of polydomain and single-domain PTO crystals allows the discussion of the importance and different origins of the so-called quasimodes, which can significantly affect the correctness of a stress analysis via Raman bands, (ii) that ion-beam milling, used for studying interfacial strain via transmission electron microscopy (TEM), can induce significant modifications of the Raman signature and thus the stress in ferroelectric thin films, and (iii) that the E(3TO) hard mode is more reliable for the estimation of biaxial residual stress by using hydrostatic pressure data than the commonly used E(1TO) soft mode.

II. EXPERIMENTAL DETAILS

Polydomains (100)/(001) and single-domain (100)-oriented PTO single crystals were grown from TiO_2-PbO-B_2O_3 flux, and the single-domain state was achieved by applying an electric field.[25] The former contains 90° domains (just as our thin films[26]) and the latter is twin free.

PTO film depositions were carried out in a vertical hot wall pulsed injection metal-organic chemical-vapor deposition (MOCVD) reactor described elsewhere.[27–29] Films were deposited on (00l) $LaAlO_3$ (LAO) [a_{LAO}=3.789 Å (Ref. 30)—indices refer to the pseudocubic setting], (00l) $SrTiO_3$

(STO) [a_{STO}=3.905 Å (Ref. 31)], (00*l*) MgO [a_{MgO} =4.212 Å (Ref. 32)], and *R*-plane cut sapphire (SAPH) [a_{SAPH}=3.5 Å (Ref. 33)] substrates supplied by CrysTec (Germany). Film thicknesses were measured from film cross-section micrographs obtained by scanning electron microscopy. XRD attests high-quality single-phase films. The *c* lattice parameter of the *c*-axis-oriented domains (*c* domains) was estimated from the five (00*l*) reflections observed in standard $\Theta/2\Theta$ scans with an error of ± 0.005 Å. More details concerning deposition techniques and standard sample characterization can be found elsewhere.[34,35]

Raman spectra were collected using a Jobin-Yvon/Horiba LabRam spectrometer equipped with a N_2-cooled charge coupled device (CCD) detector. Experiments were conducted in the micro-Raman mode at room temperature in backscattering geometry. The 514.5 nm line of an Ar^+ ion laser was focused to a spot size of about 1 μm using two Olympus objectives: ×100 [numerical aperture (NA=0.9)] and ×50 long working distance (LWD) (NA=0.5). The *VV* and *VH* polarization configurations referring to the polarization of the input and output light correspond to situations where these polarizations are parallel and crossed, respectively. The ratio of extinction is better than 1:100, indicating a low leakage of polarization due to the apparatus setting. Spectra were calibrated using Si spectra at room temperature.

III. RESULTS AND DISCUSSION

A. Effect of ferroelectric domain structure on Raman signature

In order to study potential depolarization effects of the laser beam resulting from domain structure, we have investigated single-domain (100) and polydomain (100)/(001) single crystals. Figure 1 presents Raman spectra recorded in parallel (*VV*) and crossed (*VH*) polarization configurations for both types of single crystals. As expected from Raman selection rules,[36] *E*(TO) modes are observed in the *VH* spectra of both crystals (Fig. 1).

In the case of the single-domain PTO single crystal, the *VV* spectra consist only of A_1(TO) modes according to Raman selection rules. B_1 mode can be detected in the *VV* polarization configuration when the light polarization is parallel to the ordinary axis (*a* axis) of the PTO crystal. The absence of the B_1 mode in *VV* spectra confirms that our single crystal consists of a single domain with the extraordinary axis (*c* axis) parallel to the polarization of the beam.

The analysis of the *VV* spectra of the polydomain (100)/(001) PTO crystals is more complex. The spectra consist not only of symmetry-allowed A_1(TO) and A_1(LO) modes but also of *E*(TO) modes. Moreover, modes with wavenumbers close to those of *E*(LO) modes are also observed; they will be labeled "*E*(LO)" modes for the moment (Fig. 1). Both *E*(TO) and *E*(LO) modes are usually observed in the *VH* configuration but the latter is forbidden in the backscattering geometry. We note that all mode profiles of the polydomain crystal are more asymmetric than those of the single-domain crystal.

The positions in wavenumbers of A_1(TO), *E*(TO), and "*E*(LO)" modes obtained from the *VV* and *VH* spectra of single-domain and polydomain crystals are given in Table I. In the single-domain crystal, they are very close to those reported by Foster *et al.*[37] In the case of the polydomain crystal, the positions of *E*(TO) modes in the *VH* spectra are also close to literature values, while those of A_1(TO), A_1(LO), *E*(TO), and "*E*(LO)" in the *VV* spectra are rather different (Table I and Fig. 1). Some of them differ by more than 10 cm^{-1} ["*E*(3LO)" and A_1(1LO)]. Moreover, the *E*(TO) modes observed in the *VV* configuration are shifted toward higher wavenumbers in comparison to modes measured in the *VH* configuration. Some depolarization effects of the laser beam due to the presence of twins and ferroelectric domains could be responsible for the presence of *E*(TO) modes, but this cannot explain the asymmetry and the shifts of the peaks. We will see that such anomalies of modes in the *VV* spectra can be explained by considering the presence of quasimodes.

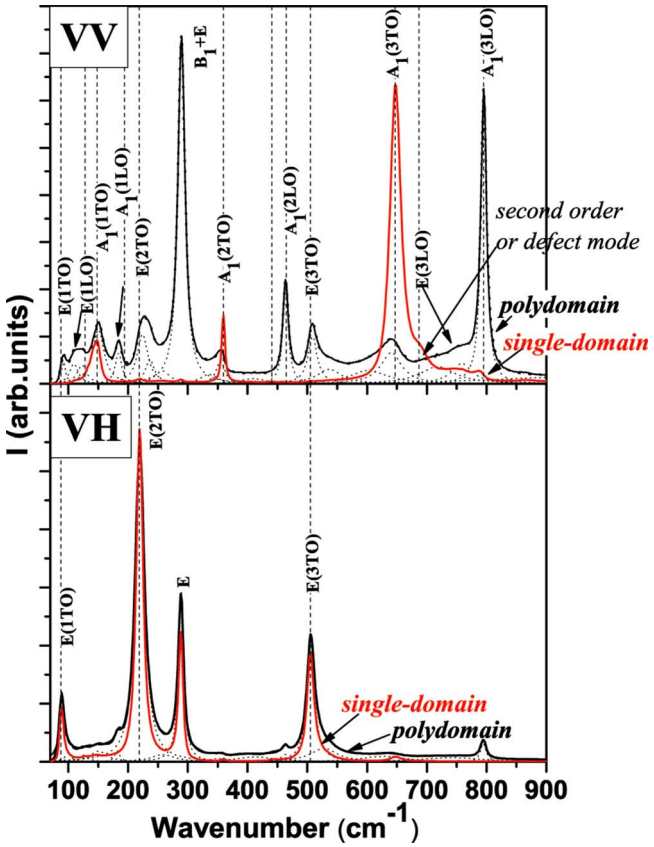

FIG. 1. (Color online) Raman spectra recorded in the *VV* and *VH* polarization configurations on polydomain (100)/(001) and single-domain (100) PTO single crystals. All modes come from the (100)-oriented (*a*-) domains except the "*E*(LO)" and A_1(LO) modes generated by the (001)-oriented (*c*-) domains. The mode wavenumbers reported by Foster *et al.* (Ref. 37) are presented as vertical dashed lines. Mode profiles in fitted spectra of polydomain PTO crystal are presented by dotted lines.

B. Origin of quasimodes in the *VV* spectra

Generally speaking, the asymmetric profiles (except for the anharmonic A_1(1TO) mode[37]), band shifts, and the pres-

TABLE I. Polydomain and single-domain $PbTiO_3$ single-crystal Raman mode wavenumbers at room temperature.

	Polarization configuration[a]	Polydomain crystal[a]	Single-domain crystal[a]	Ref. 37
E(TO)	$VH(VV)$	89.5 (92.7)	89.5	87.5
		219.9 (226.3)	219.6	218.5
		506.2 (509.0)	505.5	505
E(LO)	VV	109.3 (quasi-E)		128
				440.5
		758.2 (quasi-TO)		687
A_1(TO)	VV	150.5	148.8	148.5
		355.0	359.6	359.5
		640.7	647.8	647
A_1(LO)	VV	184.3		194
		463.9		465
		795.4		795

[a]This study.

ence of forbidden modes in Raman spectra may have several origins. They can be related to the phonon activation inside the Brillouin zone ($\mathbf{k} \neq 0$) due to a slightly disordered structure or nanosize effects. This may result in band broadening and line shift with respect to the zone-center phonon ($\mathbf{k}=0$). However, such phenomena should be observed in any configuration of polarization. The similarity of mode profiles of single-domain and polydomain crystals in the VH spectra suggests that the anomalies observed in the VV spectra may have an optical origin. We propose to relate these anomalies to the presence of quasiphonons which are expressed as additional modes at intermediate frequencies. Quasimodes are related to a so-called extraordinary wave and are observed when $0<\Theta<\pi/2$ [with Θ being the angle between the phonon wave vector $\mathbf{k}$ and the direction of the optical c axis, as illustrated in Figs. 2(a) and 2(b)]. According to the literature,[37,38] two types of quasimodes appear in our PTO spectra as a function of phonon energy.

At low wavenumbers (<200 cm^{-1}), the anisotropy in the short-range forces dominates over the long-range forces, resulting in a A_1-E splitting larger than the TO-LO splitting. Thus, E and A_1 quasimodes (quasi-E and quasi-A_1) observed

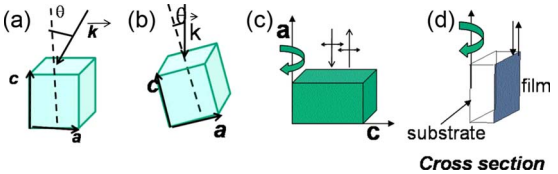

FIG. 2. (Color online) Representation of Θ angle between $\boldsymbol{k}$ and the c axis in the case of misalignments (a) in the system and (b) in the sample. Schematic representation of the rotation (c) in the case of a single crystal around its a axis and (d) in the case of a thin film around an axis parallel to the substrate plane.

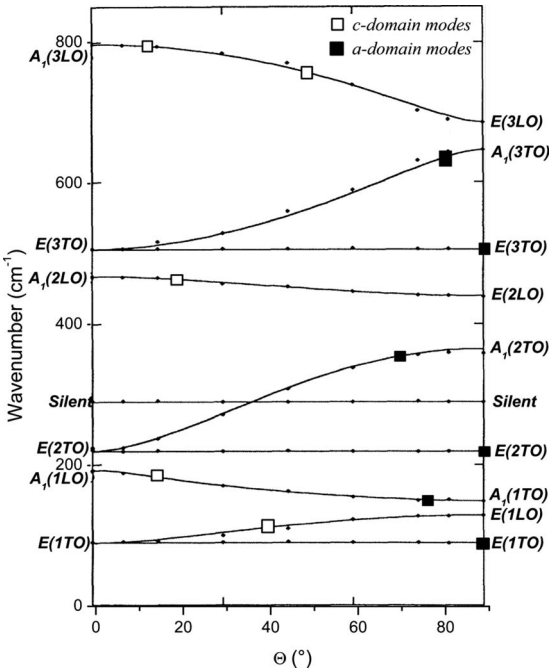

FIG. 3. Comparison of band positions of polydomain PTO single-crystal Raman modes (this study, large symbols on the curves) with PTO phonon frequency curves as a function of Θ as reported by Foster *et al.* (Ref. 37).

in a $0<\Theta<\pi/2$ configuration cannot be assigned to true TO or LO modes but are located between the wavenumbers of pure longitudinal and pure transverse E or A_1 modes.

At high wavenumbers (>200 cm^{-1}), the LO-TO splitting is much larger than the A_1-E splitting, as long-range (electrostatic) forces dominate over short-range forces. Thus, TO and LO quasimodes (quasi-TO and quasi-LO), which cannot be defined as A_1 or E modes, may appear in the spectrum when $0<\Theta<\pi/2$. Such quasimode frequencies are located between the pure E and A_1 phonon frequencies. Theoretically, quasimodes should not be observed in (001)- and (100)-oriented PTO Raman spectra, as $\Theta=0°$ and 90°, respectively.

In Fig. 3, the positions of all observed modes (Table I) are presented with respect to the angular dispersion of phonons established by Foster *et al.*[37] The mode positions measured in a VV polarization configuration correspond roughly to Foster's data obtained in the Θ range from 10 to 30° in the case of (001) domains and from 60 to 90° in the case of (100) domains, except "E(LO)" modes which occur for $\Theta=38$–48°. E(TO) mode wavenumbers in the VH spectra are not Θ dependent.

The deviation $\Delta\Theta$, which causes the presence of quasimodes in polydomain PTO single crystal or film spectra, can be due to different intrinsic and extrinsic phenomena such as the ferroelectric domain structure (discussed above), sample misalignment, objective numerical aperture, and misalignment in the spectrometer. These different origins of quasimodes will be discussed in more detail in Secs. III B 1–III B 4.

1. Sample orientation and misalignment

In agreement with the literature,[39,40] we have observed that the profiles of Raman modes of polydomain PTO in the

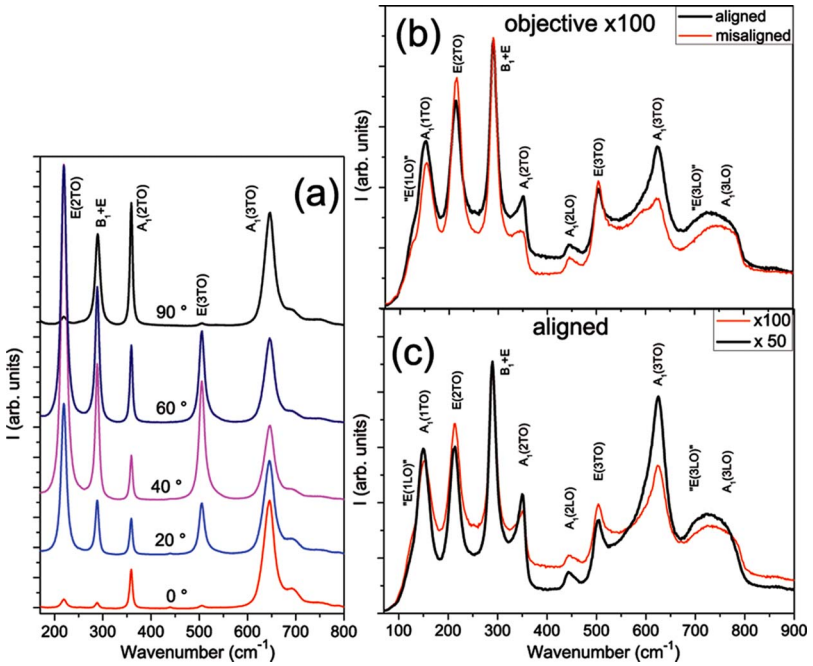

FIG. 4. (Color online) The *VV* polarized Raman spectra collected (a) from a (100) PTO single crystal at different ω angles and (b) from a (001)/(100)-oriented PTO/MgO film in the case of aligned and misaligned (turned by 20° in the (00*l*) plane) cross sections using a ×100 objective and (c) aligned samples using ×50 and ×100 objectives.

VV polarized spectra depend strongly on the sample orientation. As discussed above, the quasimodes are observed at $0 < \Theta < \pi/2$. For example, if a PTO sample is oriented along the (111) direction, the positions of Raman modes will be the wavenumbers corresponding to $\Theta = 56.4°$ on Foster's curves (Fig. 3). Thus, Raman mode positions of a stress-free sample, used as references in stress estimation, must correspond to the same Θ angle as that of the analyzed sample. This makes the stress estimation impossible in polycrystalline samples for which the different orientations of the grains result in a random distribution of Θ angles depending on the microstructure.[41,42]

To illustrate the influence of a misalignment (ω angle) between the crystal axis and light polarization, the *VV* polarized spectra were collected while rotating the (100)-oriented PTO single crystal around its *a* axis [Fig. 2(c)]. The *VV* polarized spectra, measured at different ω angles, are shown in Fig. 4(a). When $0 < \omega < \pi/2$, the E(TO) modes, allowed in the *VH* polarization configuration, are also observed in addition to A_1(TO) modes in the *VV* polarized spectrum. At $\omega = 45°$, the intensities of E(TO) modes reach a maximum. In the cases when light polarization is parallel to the *c* axis and to the *a* axis, the measured intensities of A_1(TO) modes are different. The intensities of A_1(TO) modes vary continuously from one extreme value to the other as the sample was rotated through the ω angle from 0° to 90° in extraordinary plane. If a rotation is performed in an ordinary plane, no change in A_1 mode intensities should be observed. It is important to note that quasimodes are not observed at any ω angle.

A similar experiment was performed for the polydomain sample. The Raman spectra of (001)/(100)-oriented PTO film on an MgO substrate exactly aligned with the crystallographic reference setting axes and turned about 20° in the base plane (cross section) [film optic *c* axis in the rotation plane—Fig. 2(d)] are given in Fig. 4(b). As expected, the intensities of A_1(TO) and E(TO) modes decreased and increased, respectively, while those of quasimodes remained almost unchanged. This significantly affects the mode profiles.

2. System misalignment

To study the importance of the alignment of the optical setup, we performed an experiment using a modified backscattering setup, designated as angularly resolved backscattering Raman spectroscopy. To do this, a mobile mask with a hole was placed over the scattering cone [Fig. 5(a)] and was moved to select the light to analyze near the cone center (position {3}) or on the sides (positions {2} and {4}). This experiment allowed the analysis of the scattered light at different places in the scattering cone (light coming from the sample with different angles) during the collection of the *VV* spectra of polydomain PTO single crystal. The evolution of E(1TO) mode profile for the different selections of the scat-

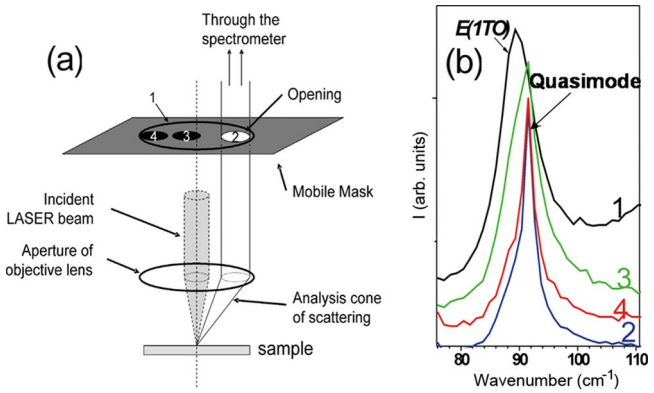

FIG. 5. (Color online) (a) The experimental setup for angularly resolved backscattering Raman spectroscopy and (b) E(1TO) soft-mode profiles collected for different selections of the scattered light in the scattering cone (×100 objective, *VV* polarization configuration).

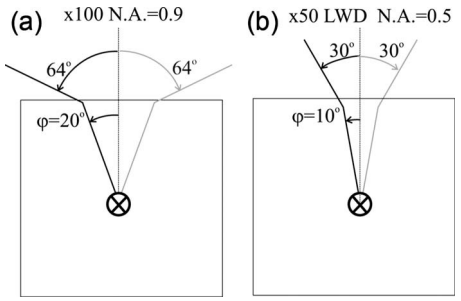

FIG. 6. Schematic representation of the angular deviation of the laser beam from backscattering geometry by using (a) ×100 and (b) ×50 objectives.

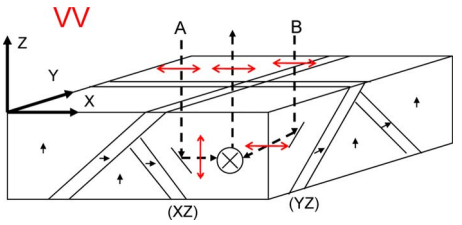

FIG. 7. (Color online) 90° scattering geometries resulting from light scattering on domain walls. A few examples of polarization configurations used for the Raman mode assignment in *a* and *c* domains in polydomain PTO single crystals and films are shown: (A) $xz/x(zx)z$ and (B) $z(xx)y/xz$.

tered light is shown in Fig. 5(b). Position {1} corresponds to the normal scattering cone without mask. It appears that the position and shape of the E(1TO) mode vary inside the scattering cone. A thorough analysis of the E(1TO) line profile provides evidence of the presence of two components under the E(1TO) line shape, which have greater separation in situations {2} and {4}, i.e., in the light scattered in the cone sides. An intense sharp line centered near 92 cm^{-1} and a shoulder near 89 cm^{-1} corresponding to the E(1TO) band position in the normal VV spectrum {1} are observed. The sharp mode is a quasi-E mode. In the central zone of the scattering cone {3}, the intensities of both modes are rather similar which leads the whole band to shift slightly toward higher wavenumbers. When the entire scattering cone is analyzed {1}, i.e., in the normal conditions to collect the VV spectra, E(1TO) is the dominant mode but it is very asymmetric and slightly shifted toward higher wavenumbers in comparison with the VH spectra due to the quasi-E mode on the high wavenumber side. Consequently, quasimodes can also appear in the VV spectra due to laser beam misalignment resulting in $\theta \neq 0°$ or 90°. However, quasimodes can still be observed in spectra even in the case of perfect alignment of the system and the sample.

3. Numerical aperture of the objective

The presence of quasimodes in relation to the numerical aperture of the objectives is now considered. The collection angles of the incident and scattered light may be varied by using objectives with different magnifications. As observed in Fig. 4(c), the VV polarized spectra of (001)/(100) PTO/MgO films collected by using LWD ×50 (NA=0.5) and ×100 (NA=0.9) objectives indicate that all mode profiles are sensitive to the numerical aperture of the objective. At high wavenumbers (>200 cm^{-1}), the E(TO) [A_1(TO)] modes are systematically shifted toward higher (lower) wavenumbers, modes become more asymmetric, and their intensities decrease in spectra collected with ×100 objective in comparison with LWD ×50 objective.

From these observations, the dependence of the incident and scattered laser beams on the numerical aperture of the objective has been considered. The angular aperture φ (NA $=\sin\varphi$) of the incident laser beam is 64° and 30° when using ×100 and LWD ×50 objectives, respectively (Fig. 6). However, when the laser light reaches the crystal or film surface, a change in the refractive index n occurs; this induces a change in the angular aperture of the incident light ($n_{air} \sin\varphi = n_{PTO} \sin\varphi_{PTO}$, where $n_{air}=1$ and $n_{PTO}=2.7$) from 64° to 20° using the ×100 objective and from 30° to 10° using the LWD ×50 objective (Fig. 6). Such an angular aperture results in an angular dispersion $\Delta\Theta=20°$ or 10°, respectively, and as a consequence, in the appearance of quasi-A_1, quasi-E, quasi-TO, and quasi-LO modes. In conclusion, the appearance of quasimodes can be reduced but not eliminated by using a LWD ×50 objective which has a lower angular aperture than the ×100 objective. Because of this, it would, in principle, be even more preferable to use a ×10 objective, but due to the enhanced optical depth of the laser beam, this leads to a significant decrease in the signal coming from the thin film. However, the presence of "E(LO)" modes, not allowed in backscattering geometry, cannot be explained by the angular aperture of the objective. It seems that more complex phenomena occur due to the ferroelectric domain structure or electric charge effects.

4. Scattering from domain walls ["E(LO)" modes]

The laser light scattering from the domain structure has also been considered. Both incident and scattered light can be reflected from a c/a domain wall probably due to charge effects before/after being scattered by phonons (Fig. 6). The c/a domain walls are tilted by 45° with respect to the crystal/film interface.[43] Thus, the reflections from such domain walls result in a 90° scattering geometry (Fig. 7) and the modes allowed in this geometry can appear in the spectra collected in the backscattering geometry (Table II). In the VH spectra E(LO) modes coming from (100)-oriented (a-) domains may be observed in addition to E(TO) modes allowed in backscattering geometry. However, the E(LO) modes, allowed in 90° scattering geometry, are not observed in the VH spectra; this suggests that the light is reflected from the domain wall mainly to the c domains (the matrix of the crystal/film). This can be explained by the fact that a domains usually form thin sheets in the c-domain matrix.[43] Thus, the contribution of a-domain modes, coming from the 90° geometry, to the VV spectra can also be neglected. Nevertheless, mode profiles in the VV spectra are affected by quasimodes coming from c domains (Table II). Quasi-E and quasi-A modes corresponding to $\Theta=45°$ can be observed at low wavenumbers <200 cm^{-1}, and quasi-LO and quasi-TO at high wavenumbers >200 cm^{-1}. As a consequence, "E(LO)" modes are

TABLE II. Predictions of modes in 90° Raman-scattering geometry resulting from reflections from domains walls. We used standard Porto notation followed by a slash indicating the polarization and propagation of light after reflection.

	VH	*HH*	*VV*
a_1 domains	$X(ZX)Y/YX$	$X(ZZ)Y/ZX$	$X(YX)Y/YX$
(100) oriented	E(TO) and E(LO)	A_1(TO)	Extinction
a_2 domains	$X(YX)Z/ZX$	$X(YY)Z/YX$	$X(ZX)X/ZX$
(010) oriented	Extinction	Quasi-A_1 or quasi-TO at $\Theta=45°$	Quasi-E, quasi-TO, and quasi-LO at $\Theta=45°$
c domains	$Z(XY)X/YZ$	$Z(YY)X/XZ$	$Z(XZ)X/XZ$
(001) oriented	Extinction	Quasi-A, quasi-TO, and quasi-LO at $\Theta=45°$	Quasi-E, quasi-TO, and quasi-LO at $\Theta=45°$

quasi-E and quasi-LO modes at low and high wavenumbers, respectively. The reflected and initial beams have the same angular dispersion resulting in a deviation of 30° from $\Theta=45°$ when using a $\times 100$ objective. In the case of the quasi-E and quasi-LO, the experimentally estimated Θ are 38 and 48° (Fig. 3). This confirms our prediction that these modes originate from c domains. Other mode profiles in the *VV* spectra are affected by the quasimode appearance due to the light scattering from domain walls as well. For example, quasi-(3TO) and quasi-(2TO) modes appear at wavenumbers lower than A_1(2TO) and A_1(3TO) modes, as expected for $\Theta=45°$ in Foster's phonon curves (Fig. 3), and result in an asymmetry of A_1(TO) mode profiles (Figs. 1 and 4). Finally, in the *VH* polarized spectra, quasimodes or modes related to reflections from domain walls are not observed because they are not allowed (Table II).

As shown above, it appears that a *VH* polarization configuration is essential to measure E(TO) modes with accuracy since quasimodes are forbidden. This condition is fundamental for stress evaluation in PTO films which is based on the E(TO) mode position. As mentioned above, A_1(TO) and A_1(LO) modes can only be obtained in the *VV* spectra; accordingly, due to the presence of quasimodes in Raman spectra of polydomain sample, their position cannot be accurately determined. Therefore, they can only be used for qualitative analysis. Quasimodes are also observed in depolarized spectra, and for the same reasons, they prevent the PTO modes from being used for stress evaluation.

Although quasimodes exist in all ferroelectrics, surprisingly, they are almost never taken into account in the current literature for the analysis of Raman scattering in ferroelectric films. Moreover, most studies on residual stress in ferroelectric films are based on Raman modes coming from depolarized spectra. For instance, the residual stress values in polycrystalline $PbZr_{1-x}Ti_xO_3$ films were determined from E(3LO) and A_1(3TO) modes.[44] The A_1(3TO) mode position is highly modified by the appearance of a quasimode in the polydomain samples, and the mode assigned to E(3LO) by other authors is a quasi-(3LO) mode with a position different from that of the real mode. In the case of polydomain PTO films deposited on compressive $NdGaO_3$ substrates, the authors assumed that the hardening (or shift toward higher wavenumbers) of the soft mode is the result of compressive misfit stress.[45] It should be remembered that the E(1TO) soft mode shifts to lower wavenumbers under compressive hydrostatic pressure as well as under tensile stress.[26] Furthermore, their study is only based on depolarized spectra without taking quasimodes into consideration, and last but not least, they used PTO single-crystal wavenumbers coming from literature. Thus, any quantitative analysis remains questionable and the shift to higher wavenumbers of the soft mode probably results at least partly from the presence of quasimodes and not from soft-mode hardening.

C. Effect of ion beam

A common technique for studying the interfacial strains is TEM. Usually, the final thinning of the samples for TEM analysis is performed by ion-beam milling. It is known that the ion-beam milling induces atomic diffusion and amorphization in the sample. Thus, it is interesting to study the ion-beam effect on the film/substrate system. The substrate was first mechanically thinned down to 5–10 μm and then low-angle ion-beam milling was used for final perforation of the sample on the substrate side (beam +8° −8° at 3.5 keV during 30–60 min) (Fig. 8). The film on the substrate did not have any direct contact with the ion beam. The Raman spec-

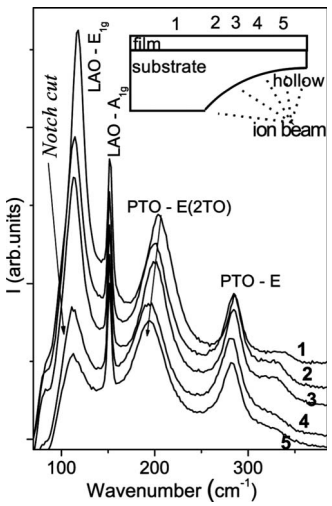

FIG. 8. Ion-beam effect on the *VH* Raman spectra of 250-nm-thick PTO/LAO film. Spectra have been recorded from five points of the film surface as shown in the inset.

tra shown in Fig. 8 were recorded from five different points of the film surface, with point 1 being the more distant from the center of the hollow and point 5 the closest as shown in Fig. 8. It appears that the Raman modes of both film and substrate are more and more shifted to lower wavenumbers as the recorded point gets closer to the center of the hollow. For instance the $E(2TO)$ mode is shifted by ~ 10 cm^{-1} at point 5. The spectra of films on substrates thinned only mechanically are identical to spectra before thinning. The shift of Raman modes to lower wavenumber in spectra of etched places may result from amorphization of the substrate and consequently of the film or from stresses created by impact of the ion beam in the substrate which would be transferred into the epitaxial film. Whatever the origin of such a Raman shift, the interpretation of the interfacial strains in samples thinned by ion-beam milling should be carried out with special care.

D. Reliability of soft and hard E(TO) modes: General considerations

The reliability of different E(TO) modes in estimating biaxial residual stress by using hydrostatic pressure data will now be considered and has already been discussed in earlier reports.[26,36] The nanosize effect on the soft and hard modes will be discussed as well.

Stresses in thin films correspond to nonhydrostatic conditions, and we have thus to introduce the effect of anisotropy in the phonon deformation potential. Supposing the E mode frequency and applied stresses can be described as follows:

$$\omega_{E(\mathrm{TO})} = a'_{E(\mathrm{TO})}(\sigma_{xx}+\sigma_{yy}) + b'_{E(\mathrm{TO})}\sigma_{zz} \pm \sqrt{c'_{E(\mathrm{TO})}(\sigma_{xx}-\sigma_{yy})^2 + d'_{E(\mathrm{TO})}(\sigma_{xy})^2}, \quad (1)$$

where $\Delta\omega_{E(\mathrm{TO})}=\omega_{E(\mathrm{TO})}-\omega_{0E(\mathrm{TO})}$, $a'_{E(\mathrm{TO})}$, $b'_{E(\mathrm{TO})}$, $c'_{E(\mathrm{TO})}$, and $d'_{E(\mathrm{TO})}$ are phonon deformation potential constants expressed in terms of compliance, and σ_{XX}, σ_{YY}, and σ_{ZZ} are stresses along a, b, and c axes of the tetragonal PTO unit cell, respectively. $c'_{E(\mathrm{TO})}$ is related to the split of double degenerate E(TO). If the a and b axes are affected by different stresses or the ab plane is under shear stresses, the E(TO) mode splits into two components. However, $c'_{E(\mathrm{TO})}$ is usually quite small and the split of the E(TO) modes is difficult to observe.

Raman modes shift linearly under biaxial stress and hydrostatic pressure;[36] only the relation coefficients differ. The evolution of the E(TO) mode wavenumber with hydrostatic pressure P ($\sigma_{XX}=\sigma_{YY}=\sigma_{ZZ}=P$) can be written as

$$\Delta\omega_{E(\mathrm{TO})} = (2a'_{E(\mathrm{TO})} + b'_{E(\mathrm{TO})})P. \quad (2)$$

Epitaxial PTO films, grown on cubic substrates, are under biaxial stress σ_b in the substrate plane. Thus, $\sigma_{XX}=\sigma_{YY}=\sigma_b$ and the shift of E(TO) modes due to biaxial stress in c domains can be expressed as

$$\Delta\omega_{E(\mathrm{TO})} = 2a'_{E(\mathrm{TO})}\sigma_b. \quad (3)$$

Thus, the absolute values of biaxial stress cannot be estimated from hydrostatic pressure data when the $a'[E(\mathrm{TO})]$ and $b'[E(\mathrm{TO})]$ coefficients are unknown.

In the literature, the stress values in tensile-strained PTO films are often estimated from the shift of the E(1TO) soft mode using hydrostatic pressure data.[46–50] However, its pressure coefficient is experimentally known only for compression (hydrostatic pressure $\partial\omega_{E(1\mathrm{TO})}/\partial P = -5.8\pm0.2$ cm^{-1} GPa^{-1}) and the soft mode is by definition anharmonic. Therefore, its behavior under tensile stress cannot be predicted and Eq. (3) becomes more complex for anharmonic modes. The E(3TO) mode is a real (harmonic) hard mode in the sense that its pressure coefficient is positive ($\partial\omega_{E(3\mathrm{TO})}/\partial P = +7.1\pm1.0$ cm^{-1} GPa^{-1}). Therefore, $\omega(P)$ can be linearly extrapolated to the tensile stress side.

Thin films are usually subjected not only to stresses but also to nanosize grain effects. As mentioned above, the condition of conservation of wave vector $\mathbf{k}$ has to be considered with some care in the case of nanostructures (for example, nanoparticles, nanothin films, a domains, which are nanosheets in the c-domain matrix, and nanograin size in thin films).[51] This effect of confinement results in the asymmetry of the profile or a shift of the soft mode to higher wavenumbers. Furthermore, field effect and the decreased tetragonality (and thus T_c) results in the shift to lower wavenumbers of the E(1TO) soft mode in the case of PTO nanoparticles.[52] In the case of hard modes, both effects usually just result in the increase in the peak width.

In addition to the choice of the correct Raman mode and on the base of Raman selection rules, Raman spectra should be collected on the film cross section to obtain information about c domains, which usually form the film matrix. Measurements on the film surface give information about a domains only and these domains are thin and might thus present size effects.

E. Illustrations

In order to test the validity of our approach to use a hard mode and not a soft mode in residual stress estimation, stress value calculations were performed from the shift of the E(1TO) soft mode and the E(3TO) hard mode. Furthermore, this analysis has been undertaken only for the VH spectra allowing the suppression of the problems related to quasimodes illustrated above. The residual stress was estimated in 250-nm-thick films on different substrates: polydomain ($c/a/c/a$ domain state) epitaxial PTO films on MgO, LAO, and STO substrates and polycrystalline films on a SAPH substrate. As seen in Table III, the E(1TO) soft mode and the E(3TO) hard mode (measured in the VH spectra on the film cross section) of c domains in films are observed well below the mode wavenumbers in bulk PTO (polydomain PTO single crystal was used as a reference). This observation suggests that PTO films are under tensile stress whatever the substrate, which is in agreement with XRD results (Fig. 9).[26] For more details on biaxial stress estimation from XRD data see Ref. 26.

Stress values were calculated from E(3TO) and E(1TO) mode wavenumbers using Eq. (2) and reported as a function of the film misfit strain in Fig. 9. For comparison, stress values obtained from lattice parameters measured by XRD are also given in Fig. 9. In epitaxial films, stress values esti-

TABLE III. Wavenumbers of E(1TO) and E(3TO) modes in the *VH* spectra of polydomain PTO single crystal and 250-nm-thick PTO films on SAPH, MgO, LAO, and STO substrates (spectra were collected on film cross sections).

	Wavenumber (cm^{-1})	
Sample	E(1TO)	E(3TO)
Polydomain PTO single crystal	89.5	506.2
PTO/SAPH	83	504.3
PTO/MgO	86.2	502.4
PTO/LAO	87	502.0
PTO/STO	88.3	504.0

mated from the shift of E(3TO) are in good agreement with XRD values. This allows us to consider that Eq. (2) can be used for the quantitative stress estimation from E(3TO) mode wavenumbers (as $a'[E(3TO)] \gg b'[E(3TO)]$) in the case of epitaxial PTO films. In this case, Raman data obtained from hydrostatic pressure experiments can thus provide an understanding and reasonable estimate of the stress state from the E(3TO) hard mode (in the *VH* polarized spectra) of *c* domains in PTO films. On the other hand, stress values obtained from the E(1TO) soft mode differ from those calculated from the XRD data which allows us to conclude that the anharmonic E(1TO) soft mode should not be used for an accurate evaluation of the residual stress in epitaxial polydomain $PbTiO_3$ thin films.

The different estimates carried out for polycrystalline PTO/SAPH films show distinct stress values (Fig. 9). In polycrystalline films (as in a powder), the grains present different crystallographic orientations, which results in a maximal dispersion of Θ angles. Therefore, the spectrum of polycrystalline samples also contains quasimodes. In other words, the projection of Foster's curves is expected to lead to a high asymmetry of the observed modes. Furthermore, the Raman selection rules are not conserved in polycrystalline films. Thus, the E(3TO) mode profile is also significantly modified by related quasimodes even in the *VH* spectra. Therefore, the E(3TO) hard-mode position is shifted upward, and thus, the stress values estimated from this mode are lower than values obtained from the lattice parameters. Accordingly, residual stress values cannot be estimated from E(TO) Raman modes in polycrystalline PTO films. It is also important to note that for the same reason the Raman mode wavenumbers of PTO powder cannot be used as reference in estimates of residual stress.

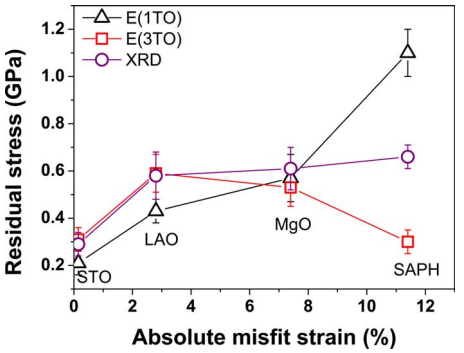

FIG. 9. (Color online) Residual stress evolution with absolute misfit strain in *c* domains of 250-nm-thick PTO films on different substrates.

IV. CONCLUSIONS

Conventional and angularly resolved Raman analysis of a stress-free polydomain and single-domain PTO single crystals revealed that phonon mode profiles of polydomain samples can be significantly modified by the existence of quasimodes in the *VV* polarized and depolarized Raman spectra. Our results illustrate that the use of the *VH* configuration of polarization and the consideration of quasimodes are essential to obtain spectra, allowing an accurate estimation of residual stress values. Moreover, residual stress values in polycrystalline films cannot be estimated from Raman modes as the spectra are perturbed by relaxed Raman selection rules and quasimodes. Sample thinning by ion beam may create additional stresses or amorphize the substrate and the sample, which may give rise to errors in the interpretation of interfacial strains in the film by TEM analysis. It has been shown that Raman scattering is a versatile probe to test the existence of such stresses.

In the literature, the residual stress in PTO films is mainly analyzed by considering the shift of the E(1TO) soft mode. We argue that this choice is questionable because of the anharmonic nature of the soft mode and possible nanosize and field effects. As a consequence, we highlight and apply an alternative analysis based on the behavior of the E(3TO) mode which is a hard mode and possibly the only mode usable for such a stress determination. Residual stress values obtained from the E(3TO) mode in the *VH* geometry are consistent with those calculated from lattice parameters derived from the XRD data.

ACKNOWLEDGMENTS

We would like to thank K. Wojcik for the $PbTiO_3$ crystal growth. This work was financially supported by the European network of excellence FAME and EGIDE.

*Corresponding author: a.bartasyte1@physics.ox.ac.uk

[1] J. F. Scott, Science **315**, 954 (2007).
[2] K. J. Choi, M. Biegalski, Y. L. Li, A. Sharan, J. Shubert, R. Uecker, P. Reiche, Y. B. Chen, X. Q. Pan, V. Gopalan, L.-Q. Chen, D. G. Schlom, and C. B. Eom, Science **306**, 1005 (2004).
[3] J. H. Haeni, P. Irvin, W. Chang, R. Uecker, P. Reiche, Y. L. Li, S. Choudhury, W. Tian, M. E. Hawley, B. Craigo, A. K. Tagantsev, X. Q. Pan, S. K. Streiffer, L. Q. Chen, S. W. Kirchoefer, J. Levy, and D. G. Schlom, Nature (London) **430**, 758 (2004).
[4] F. He, B. O. Wells, Z.-G. Ban, S. P. Alpay, S. Grenier, S. M. Shapiro, W. Si, A. Clark, and X. X. Xi, Phys. Rev. B **70**, 235405 (2004).
[5] F. He and B. O. Wells, Appl. Phys. Lett. **88**, 152908 (2006).
[6] P.-E. Janolin, F. Le Marrec, J. Chevreul, and B. Dkhil, Appl. Phys. Lett. **90**, 192910 (2007).
[7] P.-E. Janolin, B. Fraisse, F. Le Marrec, and B. Dkhil, Appl. Phys. Lett. **90**, 212904 (2007).
[8] Yu. I. Yuzyuk, P. Simon, I. N. Zakharchenko, V. A. Alyoshin, and E. V. Sviridov, Phys. Rev. B **66**, 052103 (2002).
[9] J. A. Sanjurjo, E. Lopez-Cruz, and G. Burns, Phys. Rev. B **28**, 7260 (1983).
[10] F. Cerdeira, W. B. Holzapfel, and D. Bauerl, Phys. Rev. B **11**, 1188 (1975).
[11] M. Ahart, M. Somayazulu, R. E. Cohen, P. Ganesh, P. Dera, H.-k. Mao, R. J. Hemley, Y. Ren, P. Liermann, and Z. Wu, Nature (London) **451**, 545 (2008).
[12] H. Zheng, J. Kreisel, Y. H. Chu, R. Ramesh, and L. Salamanca-Riba, Appl. Phys. Lett. **90**, 113113 (2007).
[13] I. A. Kornev, L. Bellaiche, P. Bouvier, P. E. Janolin, B. Dkhil, and J. Kreisel, Phys. Rev. Lett. **95**, 196804 (2005).
[14] I. A. Kornev and L. Bellaiche, Phase Transitions **80**, 385 (2007).
[15] G. A. Samara and E. L. Venturini, Phase Transitions **79**, 21 (2006).
[16] G. Irmer and M. Jurich, Phys. Status Solidi A **204**, 2309 (2007).
[17] Z. Q. Xu, L. Lev, M. Lukitsch, and A. Kumar, J. Mater. Res. **22**, 1012 (2007).
[18] G. Pezzotti, Expert Rev. Med. Devices **4**, 165 (2007).
[19] A. M. Limarga and D. R. Clarke, J. Am. Ceram. Soc. **90**, 1272 (2007).
[20] R. A. Forman, G. J. Piermarini, J. D. Barnett, and S. Block, Science **176**, 284 (1972).
[21] S. Margueron and D. R. Clarke, Acta Mater. **54**, 5551 (2006).
[22] T. Sakashita, M. Deluca, S. Yamamoto, H. Chazono, and G. Pezzotti, J. Appl. Phys. **101**, 123517 (2007).
[23] M. S. Amer, J. Maguire, L. Cai, R. Biggers, J. Busbee, and S. R. Leclair, J. Appl. Phys. **89**, 8030 (2001).
[24] X. Zhang, Y. Liu, and S. Chen, J. Raman Spectrosc. **36**, 1101 (2005).
[25] K. Wojcik, Ferroelectrics **82**, 25 (1988).
[26] A. Bartasyte, O. Chaix-Pluchery, J. Kreisel, M. Boudard, C. Jimenez, A. Abrutis, Z. Saltyte, and F. Weiss, J. Appl. Phys. **103**, 014103 (2008).
[27] J. P. Senateur, F. Weiss, O. Thomas, R. Madar, and A. Abrutis, Patent No. FR 2707 671 (1993).
[28] F. Weiss, J. Lindner, J. P. Sénateur, C. Dubourdieu, V. Galindo, M. Audier, A. Abrutis, M. Rosina, K. Frohlich, W. Haessler, S. Oswald, A. Figueras, and J. Santiso, Surf. Coat. Technol. **133-134**, 191 (2000).
[29] J. P. Sénateur, C. Dubourdieu, F. Weiss, M. Rosina, and A. Abrutis, Adv. Mater. Opt. Electron. **10**, 155 (2000).
[30] S. A. Hayward, F. D. Morrison, S. A. T. Redfern, E. K. H. Salje, J. F. Scott, K. S. Knight, S. Tarantino, A. M. Glazer, V. Shuvaeva, P. Daniel, M. Zhang, and M. A. Carpenter, Phys. Rev. B **72**, 054110 (2005).
[31] G. M. Meyer, R. J. Nelmes, and J. Hutton, Ferroelectrics **21**, 461 (1978).
[32] ICDD Report No. 00-045-0946 (unpublished).
[33] T. Huang, W. Parish, N. Masciocchi, and P. Wang, Adv. X-Ray Anal. **33**, 295 (1990).
[34] A. Bartasyte, A. Abrutis, C. Jimenez, F. Weiss, O. Chaix-Pluchery, and Z. Saltyte, Ferroelectrics **353**, 104 (2007).
[35] A. Bartasyte, R. Bouregba, E. Dogheche, M. Boudard, G. Poullain, C. Jimenez, V. Plausinaitiene, D. Remiens, A. Abrutis, F. Weiss, O. Chaix-Pluchery, and Z. Saltyte, Surf. Coat. Technol. **201**, 9340 (2007).
[36] A. Bartasyte, O. Chaix-Pluchery, J. Kreisel, J. Santiso, S. Margueron, M. Boudard, C. Jimenez, A. Abrutis, and F. Weiss, IEEE Trans. Ultrason. Ferroelectr. Freq. Control **54**, 2623 (2007).
[37] C. M. Foster, Z. Li, M. Grimsditch, S.-K. Chan, and D. J. Lam, Phys. Rev. B **48**, 10160 (1993).
[38] C. A. Arguello, D. L. Rousseau, and S. P. S. Porto, Phys. Rev. **181**, 1351 (1969).
[39] M. Deluca, T. Sakashita, and G. Pezzotti, Appl. Phys. Lett. **90**, 051919 (2007).
[40] J. C. Gonzalez, N. Mestres, T. Puig, J. Gazquez, F. Sandiumenge, X. Obradors, A. Usoskin, Ch. Jooss, H. C. Freyhardt, and R. Feenstra, Phys. Rev. B **70**, 094525 (2004).
[41] W. J. Brya, Phys. Rev. Lett. **26**, 1114 (1971).
[42] G. Burns and B. A. Scott, Phys. Rev. Lett. **25**, 1191 (1970).
[43] C. S. Ganpule, V. Nagarajan, B. K. Hill, A. L. Roytbard, E. D. Willians, S. P. Alpay, A. Roelops, R. Waser, and L. M. Eng, J. Appl. Phys. **91**, 1477 (2002).
[44] J. Cheng, L. He, S. Yu, and Z. Meng, Appl. Phys. Lett. **88**, 152906 (2006).
[45] L. Sun, Y. F. Chen, L. He, C.-Z. Ge, D.-S. Ding, T. Yu, M.-S. Zhang, and N. B. Ming, Phys. Rev. B **55**, 12218 (1997).
[46] D. Valim, A. G. Sauza Filho, P. T. C. Freire, J. Mendes Filho, C. A. Guavany, R. N. Reispaud, and E. B. Araujo, J. Phys. D **37**, 744 (2004).
[47] D. Fu, T. Ogawa, H. Suzuki, and K. Ishikawa, Appl. Phys. Lett. **77**, 1532 (2000).
[48] P. S. Dobal, S. Bhaskar, S. B. Majamder, and R. S. Katiyar, J. Appl. Phys. **86**, 828 (1999).
[49] S.-H. Lee, H. M. Jang, S. M. Cho, and G.-C. Yi, Appl. Phys. Lett. **80**, 3165 (2002).
[50] T. Ohno, D. Fu, H. Suzuki, H. Migazaki, and K. Ishikawa, J. Eur. Ceram. Soc. **24**, 1669 (2004).
[51] W. H. Weber and R. Merlin, *Raman Scattering in Materials Science* (Springer-Verlag, Berlin, 2000).
[52] K. Ishikawa, K. Yoshikawa, and N. Okada, Phys. Rev. B **37**, 5852 (1988).